Experimental realization of KPZ dynamics: Slow combustion of paper

Markko Myllys[1], J. Maunuksela, J. Merikoski, T. Ala-Nissilä, M.J. Alava, N. Provatas , J. Kuittu, O-P. Kähkönen, M. Avikainen, M. K. Horvath, M. Ha, M den Nijs ,T. Kärkkäinen, M. S. Welling, R.J. Wijngaarden

and J. Timonen

1. University of Jyväskylä, Finland

Outline

I. Slow combustion
II. Experimental set-up
III. Demonstration of KPZ dynamics
IV. Future work

References:

[1] MAUNUKSELA, J., MYLLYS, M., KÄHKÖNEN, O.-P., TIMONEN, J., PROVATAS, N., ALAVA, M. J., AND ALA-NISSILA, T., **Kinetic Roughening in Slow Combustion of Paper.** Phys. Rev. Lett. **79** (1997) 1515–1518.

[2] MAUNUKSELA, J., MYLLYS, M., TIMONEN, J., KUITTU, M., ALANISSILA, T., ALAVA, M. J., AND PROVATAS, N., **Reply to the Comment of Amaral and Makse.** Phys. Rev. Lett. **80** (1998) 5707.

[3] MAUNUKSELA, J., MYLLYS, M., TIMONEN, J., ALAVA, M.J., AND ALANISSILA, T., **Kardar-Parisi-Zhang Scaling in Kinetic Roughening of Fire Fronts.** Physica A **266** (1999) 372–376.

[4] MYLLYS, M., MAUNUKSELA, J., ALAVA, M.J., ALA-NISSILA, T., AND TIMONEN, J., **Scaling and Noise in Slow Combustion of Paper.** Phys. Rev. Lett. **84** (2000) 1946–1949.

[5] MYLLYS, M., MAUNUKSELA, J., ALAVA, M., ALA-NISSILA, A., MERIKOSKI, J., AND TIMONEN, J**., Kinetic Roughening in Slow Combustion of Paper.** Phys. Rev. E **64** (2001) 036101.

[6] MERIKOSKI, J., MAUNUKSELA, J., MYLLYS, M., TIMONEN, J., AND ALAVA, M. J., **Temporal and Spatial Persistence of Combustion Fronts.** Phys. Rev. Lett. **90** (2003) 024501.

[7] MAUNUKSELA, J., MYLLYS, M., MERIKOSKI, J., TIMONEN, J., KÄRKKÄINEN, T., WELLING, M. S., AND WIJNGAARDEN, R. J., **Determination of the Stochastic Evolution Equation from Noisy Experimental Data.** Eur. Phys. J. B **33**, 193–202 (2003)

[8] MYLLYS, M., MAUNUKSELA, J., MERIKOSKI, J., TIMONEN, J., AND AVIKAINEN, M., **KPZ equation with realistic short-range correlated noise.**
Eur. Phys. J. B **36**, 619–626 (2003)

[9] MYLLYS, M., MAUNUKSELA, J., MERIKOSKI, J., TIMONEN, J., HA, M., AND DEN NIJS, M., **Effect of a columnar defect on the shape of slow combustion fronts.** PHYSICAL REVIEW E **68**, 051103 (2003)

[10] MIETTINEN, L., MYLLYS, M., MERIKOSKI, J., AND TIMONEN, J., **Experimental determination of KPZ height-fluctuation distributions**, Eur. Phys. J. B **46** (2005) 55–60.

300 mm

00:00

Slow combustion

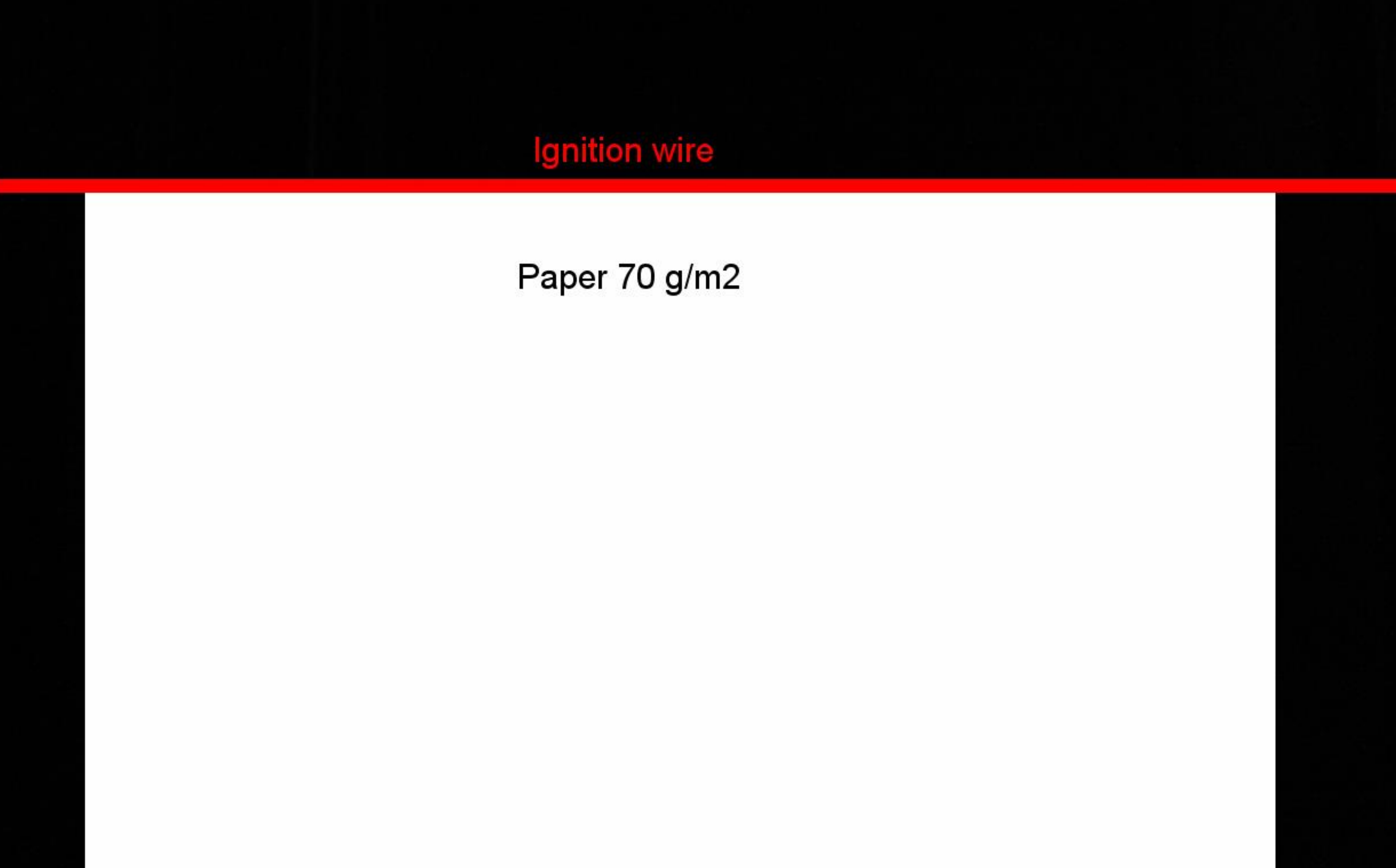

Slow combustion

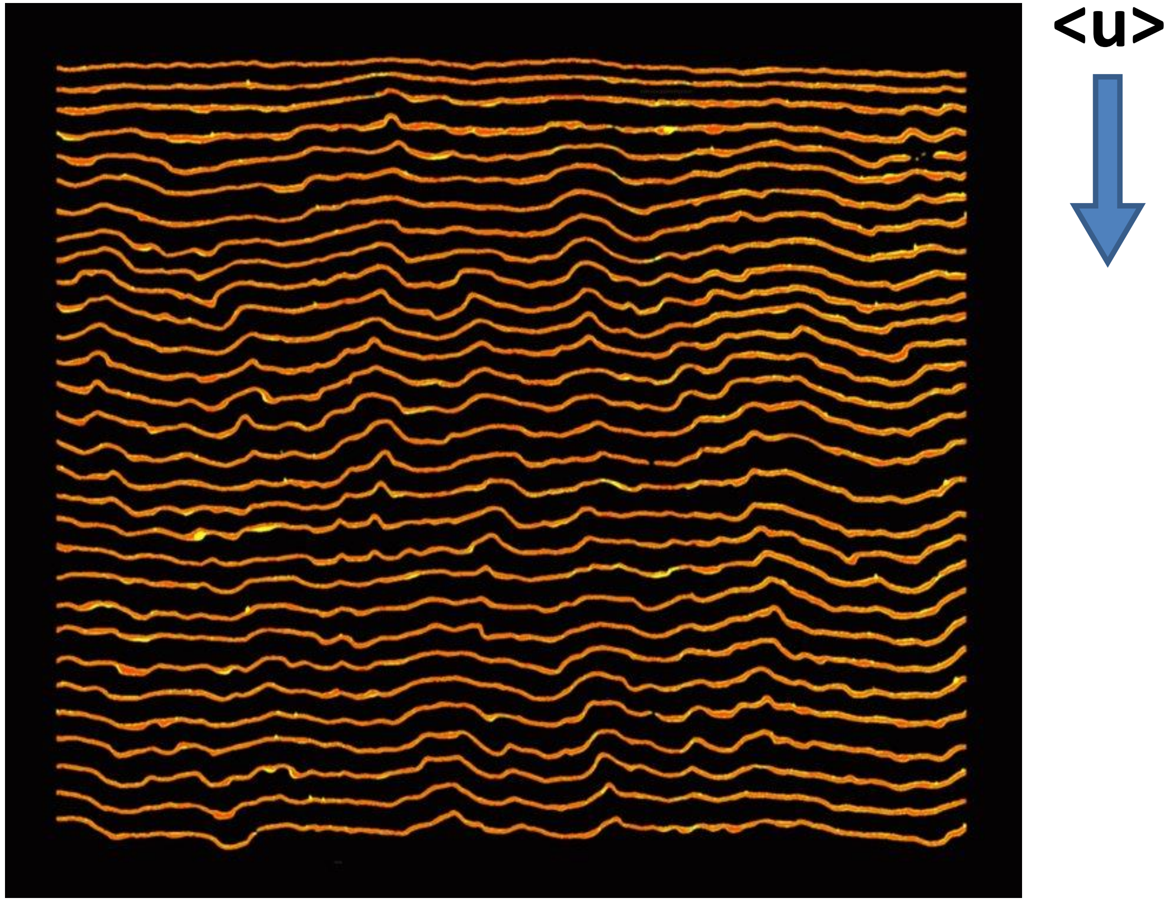

Slow combustion fronts digitized at 10 second intervals.
The width of the area is 310 mm.

Laboratory

Experimental set-up

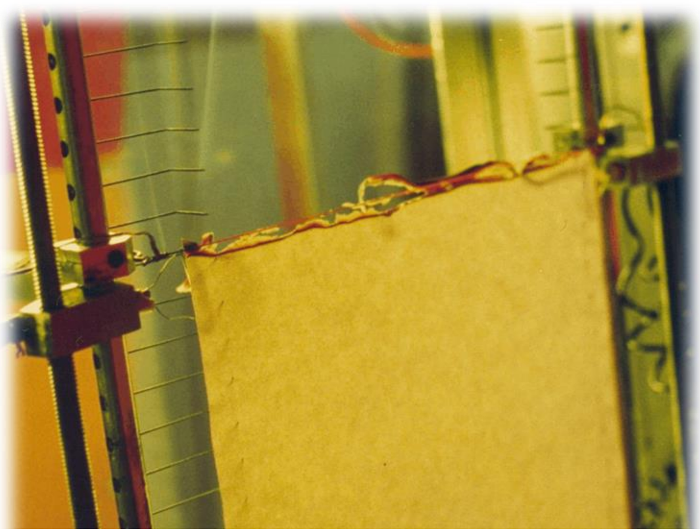

Experimental set-up

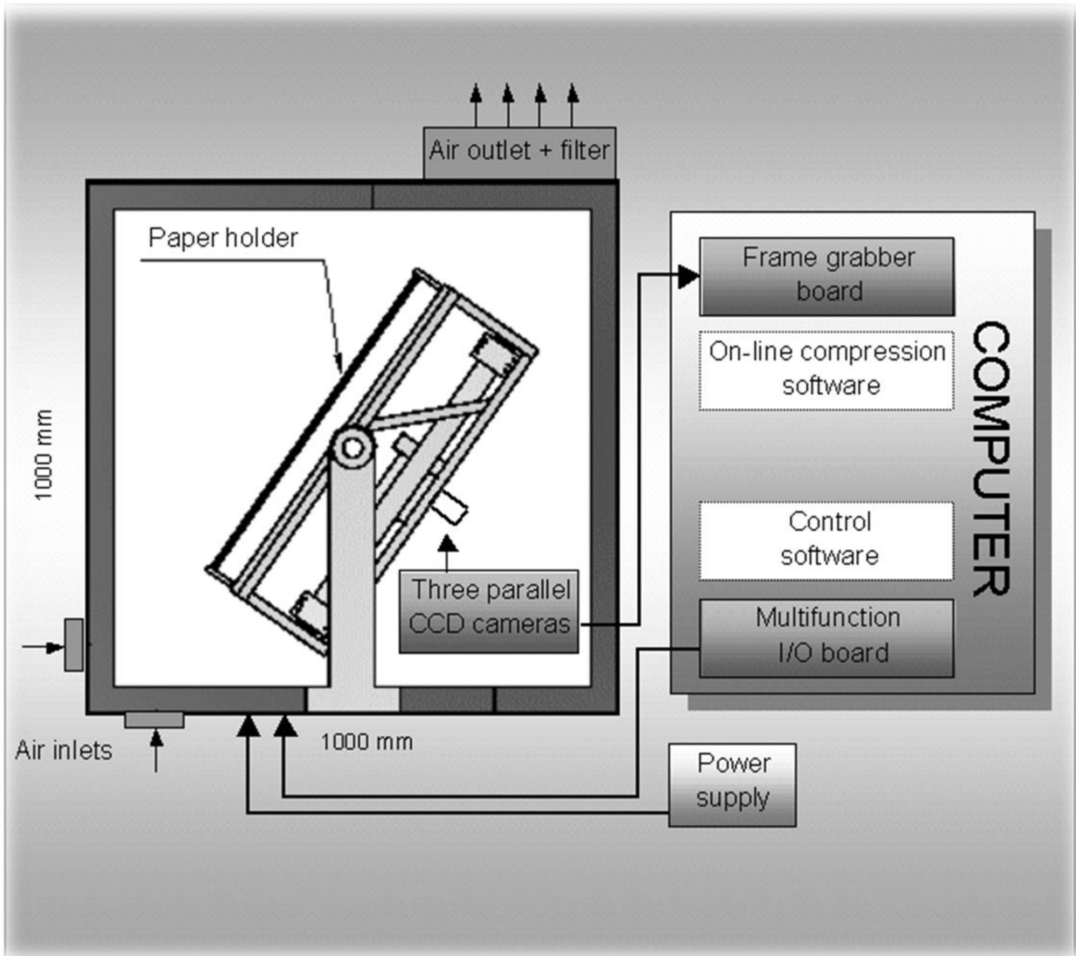

Experimental set-up

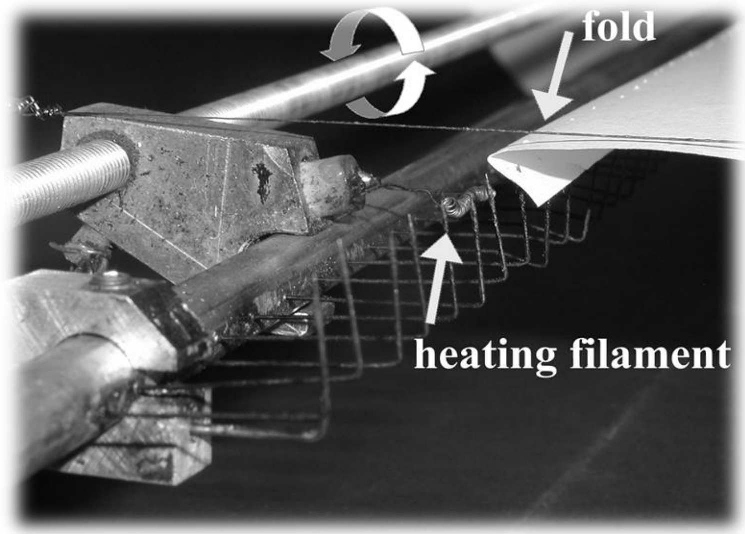

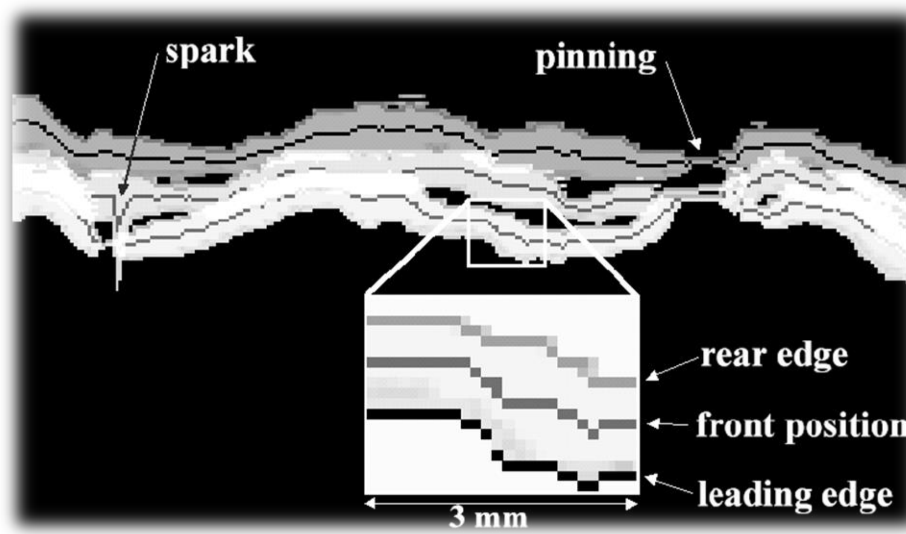

Samples

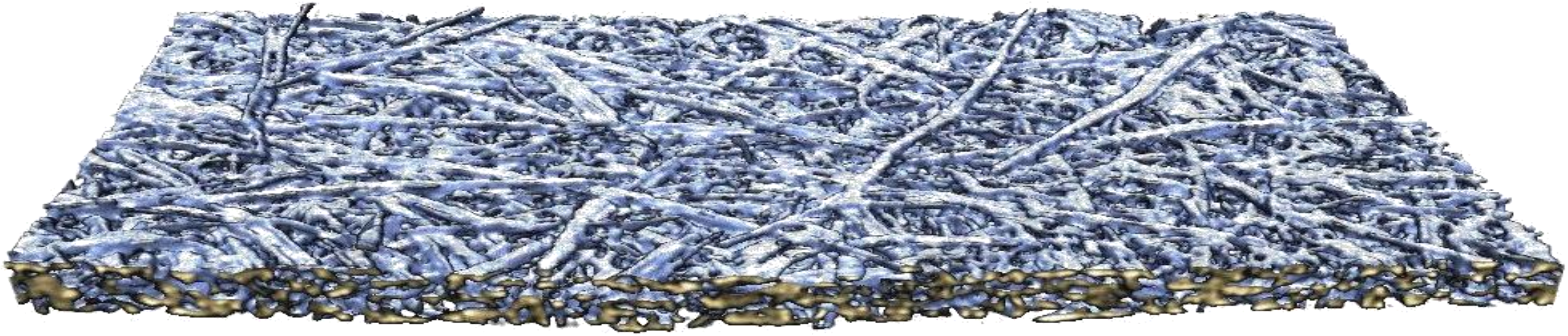

-Paper is produced by pressing together cellulose pulp
-Pulp can be made mechanically, chemically or it can be recycled
-Additional fillers may be used to enhance the properties of base paper
-A coating of kaoline or calcium carbonate may be used to impart certain surface qualities to the paper

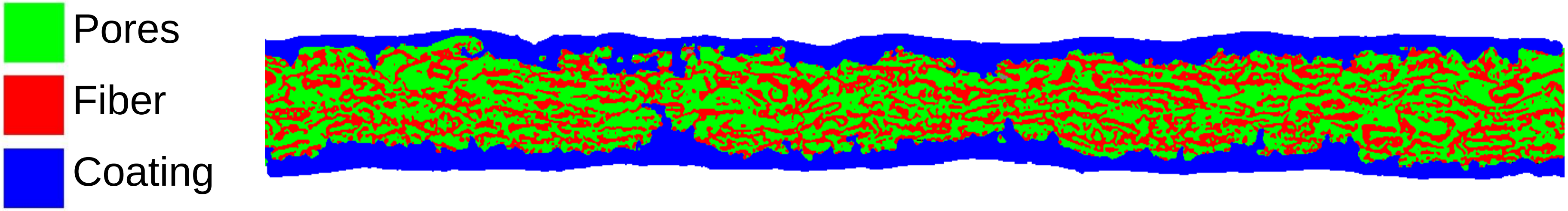

Samples

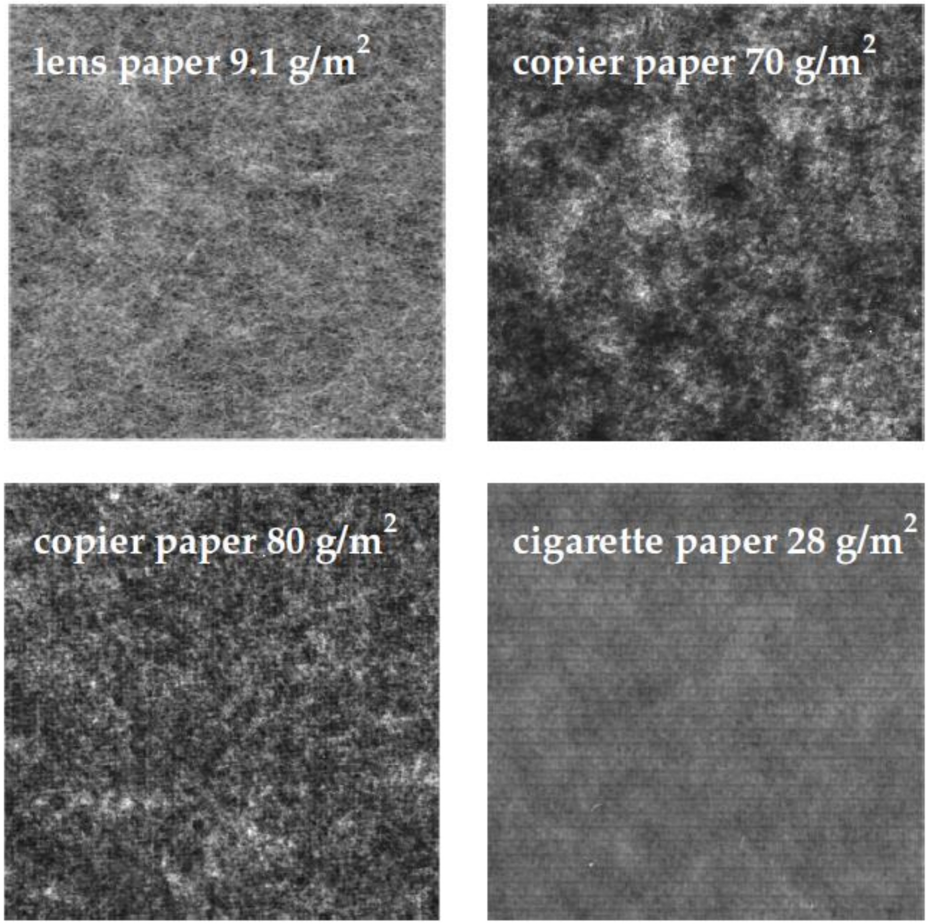

FIGURE 3.1 β-radiographs of paper samples of size (30×30) mm^2. The image of the lens paper is made by optical scanning.

$$C_m(\vec{r}) = \langle [m(\vec{x}) - \overline{m}][m(\vec{x}+\vec{r}) - \overline{m}] \rangle,$$

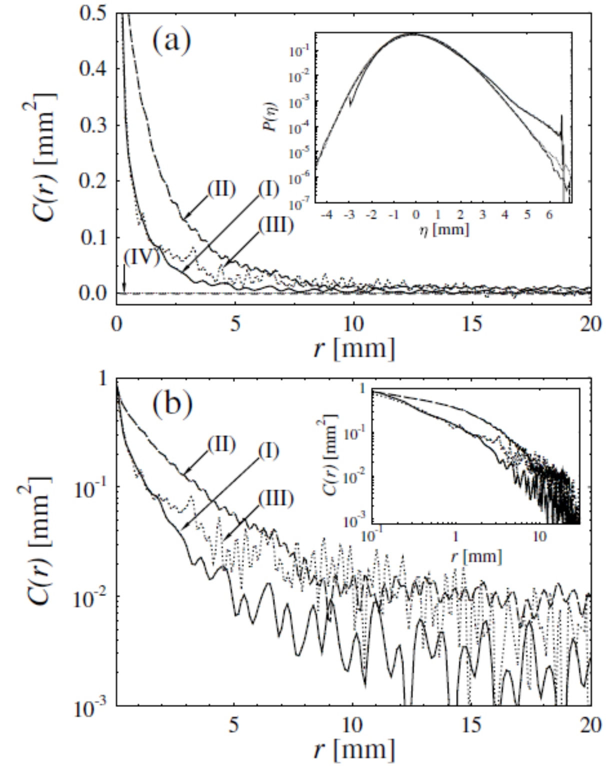

Fig. 2. The noise fluctuation correlation functions $C(r)$ for noises (II), (III), (I) and (IV) from top to bottom in linear (a) and in semi-logarithmic (b) scale. The inset of (a) shows the noise amplitude distributions and the inset of (b) a double-logarithmic plot of the correlation function.

Samples

Front velocity was controlled by KNO_3 concentration.

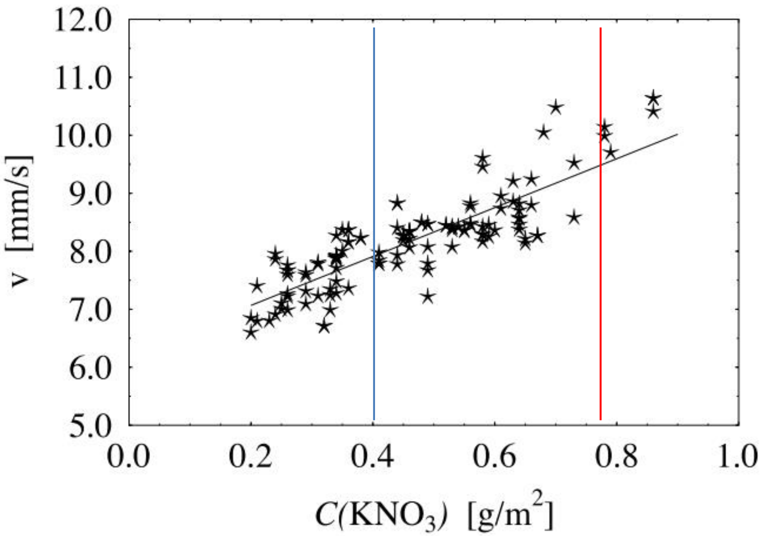

FIG. 2. Front velocity as a function of potassium-nitrate concentration. Measured points are denoted by stars and the line is a linear fit to these points.

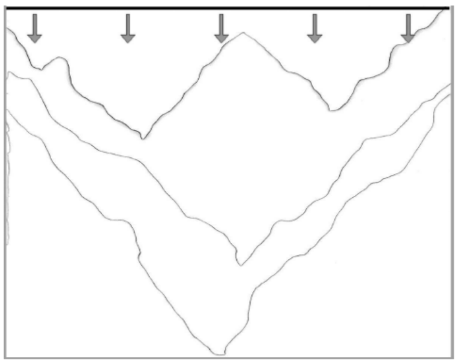

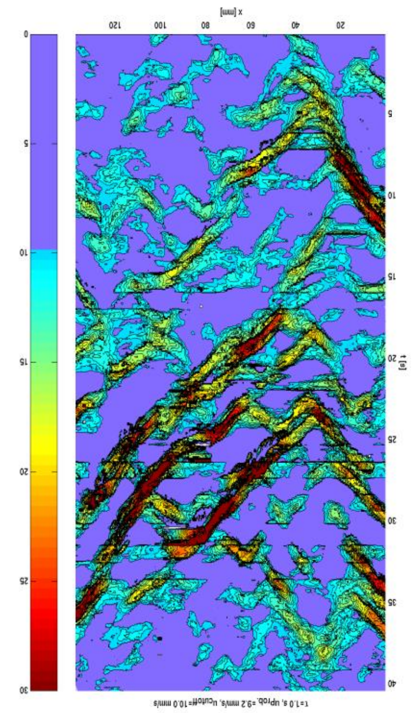

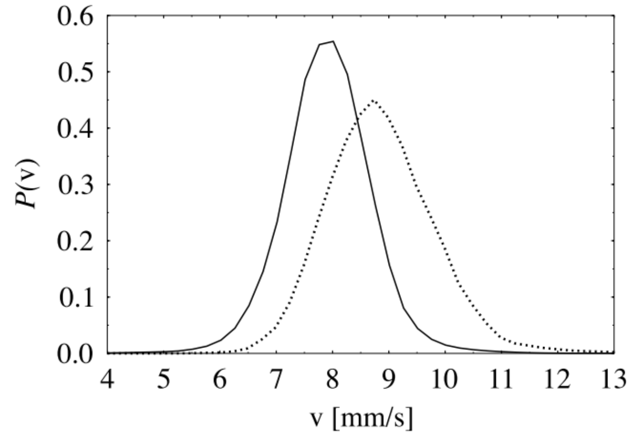

FIG. 1. Velocity distributions for slow-combustion fronts with potassium-nitrate concentrations $0.34\ \mathrm{g\,m^{-2}}$ (full line) and $0.536\ \mathrm{g\,m^{-2}}$ (dashed line). Velocities are determined for a time difference of 2 s.

Demonstration of KPZ dynamics

KPZ equation:

$$\frac{\partial h}{\partial t} = \nu \nabla^2 h + \frac{\lambda}{2}(\nabla h)^2 + c + \eta(x,t)$$

Surface width :

$$w = \sqrt{\frac{1}{L}\sum_x \left\langle \left[h(x,t) - \bar{h}(t) \right]^2 \right\rangle}$$

scales as

$$w(t,L) \sim \begin{cases} t^{\beta} & , t \ll t_{sat} \\ L^{\chi} & , t \gg t_{sat} \end{cases}$$

χ = roughening exponent

β = growth exponent

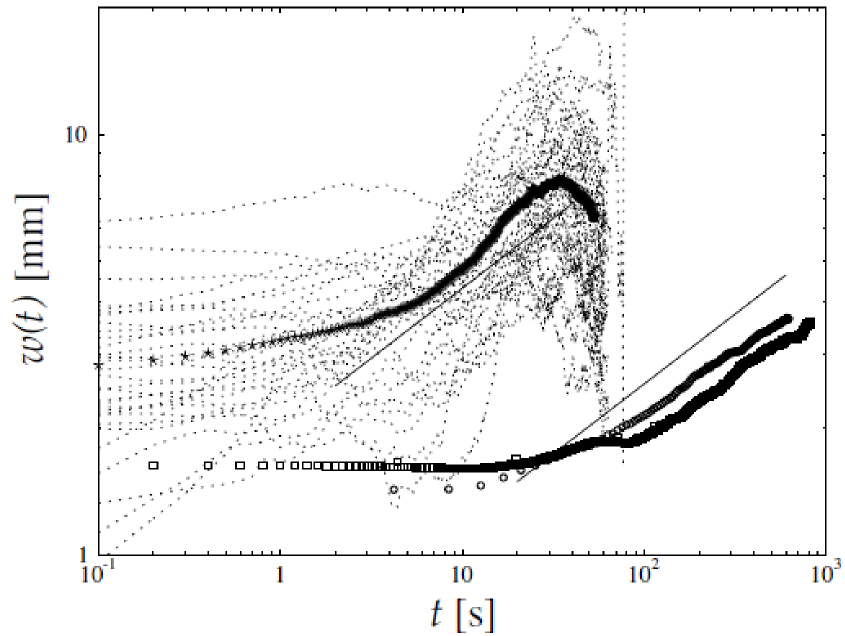

FIGURE 4.1 Time evolution of the front width for three paper grades. The slope of both solid lines is the KPZ value for the growth exponent, $\beta = 1/3$. The symbols used in the figures of this Chapter are: ★ = lens paper (9.1 g/m^2), ○ = copier paper (70 g/m^2) and □ = copier paper (80 g/m^2). Individual lens paper burns are denoted by dotted lines and the average of them by stars.

Demonstration of KPZ dynamics

KPZ equation:

$$\frac{\partial h}{\partial t} = \nu \nabla^2 h + \frac{\lambda}{2}(\nabla h)^2 + c + \eta(x,t)$$

Scaling properties from the **two-point correlation function**

$$C_2(r,t) = \left\langle \overline{[\delta h(x',t') - \delta h(x'+r,t'+t)]^2} \right\rangle$$

Asymptotically:

$$C_2(r,0) \sim A r^{2\chi} \quad \text{and} \quad C_2(0,t) \sim B t^{2\beta}$$

Universal coupling constant:

$$g^* = \frac{\lambda}{2}\left[\frac{A}{B^{z/2}}\right]^{1/\chi}$$

Theoretical prediction for KPZ equation with $\eta\,(x,t) =$ white noise:

$$\beta = 1/3, \quad \chi = 1/2$$

$$g^* = 0.87$$

Demonstration of KPZ dynamics

Spatial correlation functions

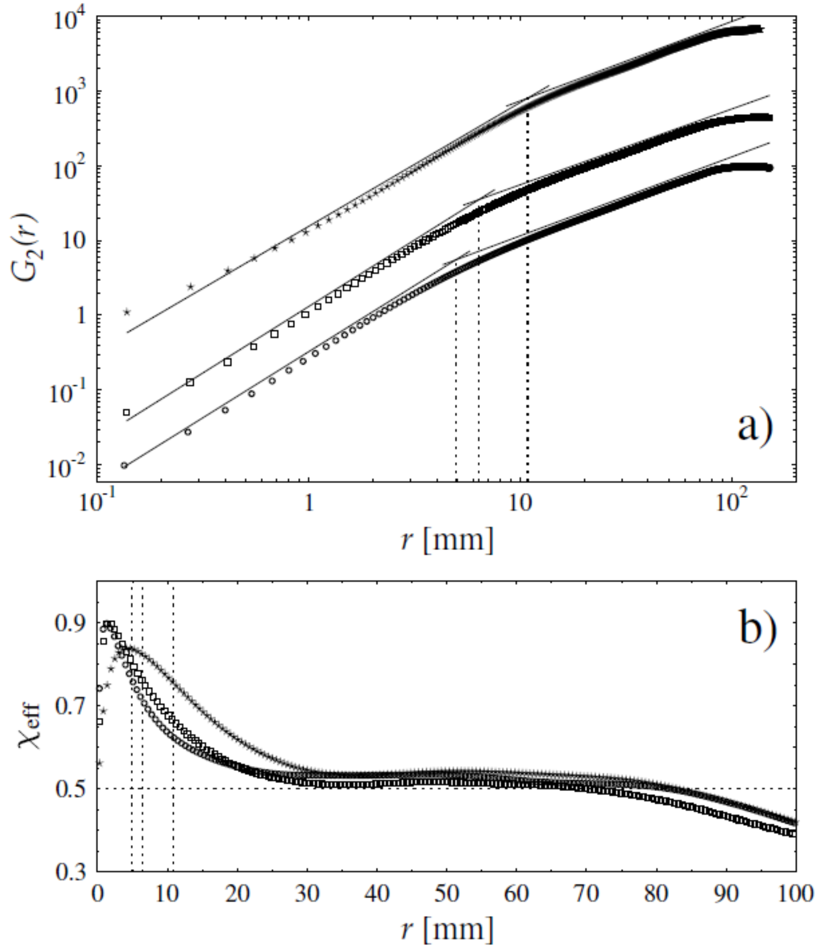

FIGURE 4.2 (a) Spatial correlation functions $G_2(r)$ for three paper grades, and (b) the resulting effective exponents. Crossover scales from the short-range regimes to the asymptotic scaling regimes are marked with dotted lines.

Demonstration of KPZ dynamics

Temporal correlation functions

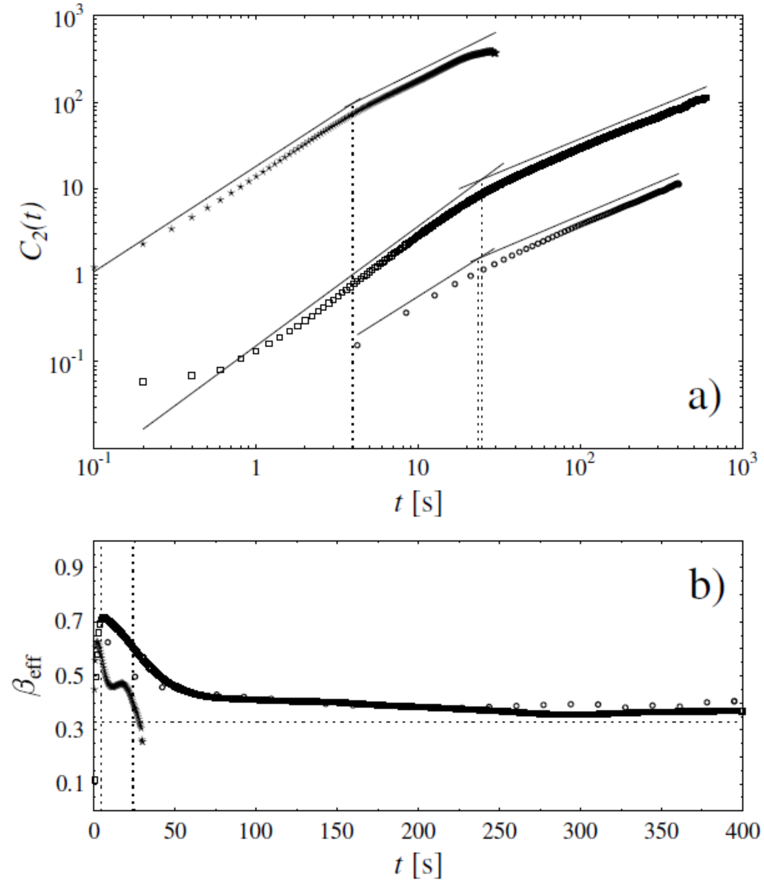

FIGURE 4.3 (a) Temporal correlation functions $C_2(t)$ for three paper grades, and (b) the resulting effective exponents. Crossover scales from the short-range regimes to the asymptotic scaling regimes are marked with dotted lines.

Demonstration of KPZ dynamics

Universal coupling constant

$$g^* = \frac{\lambda}{2}\left[\frac{A}{B^{z/2}}\right]^{1/\chi}$$

TABLE III. Results for the correlation amplitudes, λ, and the universal quantities using $\beta = 1/3$ and $\chi = 1/2$.

Paper grade	A	B	λ	R_G	g^*
70 gm^{-2}	0.52(2)	0.186(12)	0.465(2)	0.74(6)	0.79(9)
80 gm^{-2}	0.475(7)	0.14(1)	0.370(1)	0.73(5)	0.76(8)
9.1 gm^{-2}	3.4(1)	8.0(8)	4.0(4)	0.62(8)	1.0(2)

Theory : g*=0.87 [8]

[8] T. Hwa and E. Frey, Phys. Rev. A **44**, R7873 (1991).

Demonstration of KPZ dynamics

TABLE 4.1 Results for the scaling exponents, amplitudes and universal constants. The two latter quantities were determined for $\beta = 1/3$ and $\chi = 1/2$. The scaling exponents β and χ were obtained by first subtracting the intrinsic widths from the data.

	χ_{SR}	χ_{LR}	β_{SR}	β_{LR}	A	B	R_g	g^*
70 g/m^2	0.90(3)	0.50(4)		0.36(3)	0.52(2)	0.186(12)	0.74(6)	0.79(9)
80 g/m^2	0.90(4)	0.47(4)	0.75(5)	0.34(4)	0.475(7)	0.14(1)	0.73(5)	0.76(8)
9.1 g/m^2	0.85(1)	0.50(6)	0.64(3)	0.43(6)	3.4(1)	8.0(8)	0.62(8)	1.0(2)

Theoretical prediction for KPZ equation with $\eta(x,t)$ = white noise:

$$\beta = 1/3, \quad \chi = 1/2$$

$$g^* = 0.87$$

Demonstration of KPZ dynamics

Persistence

<u>Height-fluctuation field:</u>

* $\delta h(x,t) > 0$; black region

* $\delta h(x,t) < 0$; white region

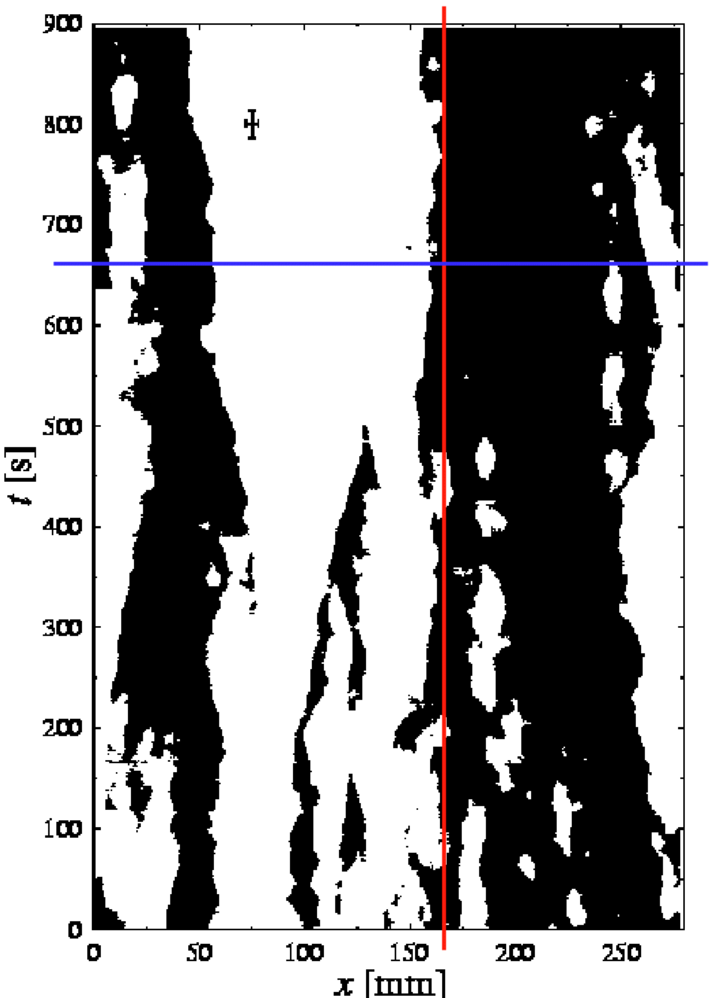

* $\delta h = h(x,t) - \bar{h}(t)$

* Temporal first-return distribution:

$f^{temp}(\tau)$ is the distribution of the return time τ defined as the time interval for which δh stays above/below zero at fixed x.

* Spatial first-return distribution:

$f^{temp}(l)$ is the distribution of l defined as the distance over which δh stays above/below zero.

* Persistence exponents θ_{temp} and θ_{spat} :

$f^{temp}(\tau) \sim \tau^{-(1+\theta_{temp})}$

$f^{spat}(\tau) \sim \tau^{-(1+\theta_{spat})}$

Demonstration of KPZ dynamics

Persistence

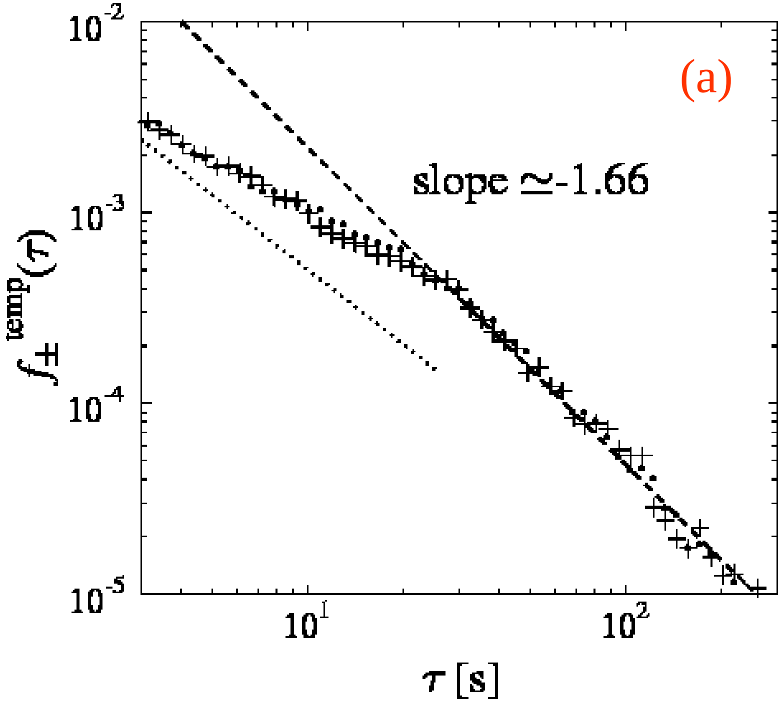

The stationary temporal first-return distributions $f^{temp}(\tau)$.

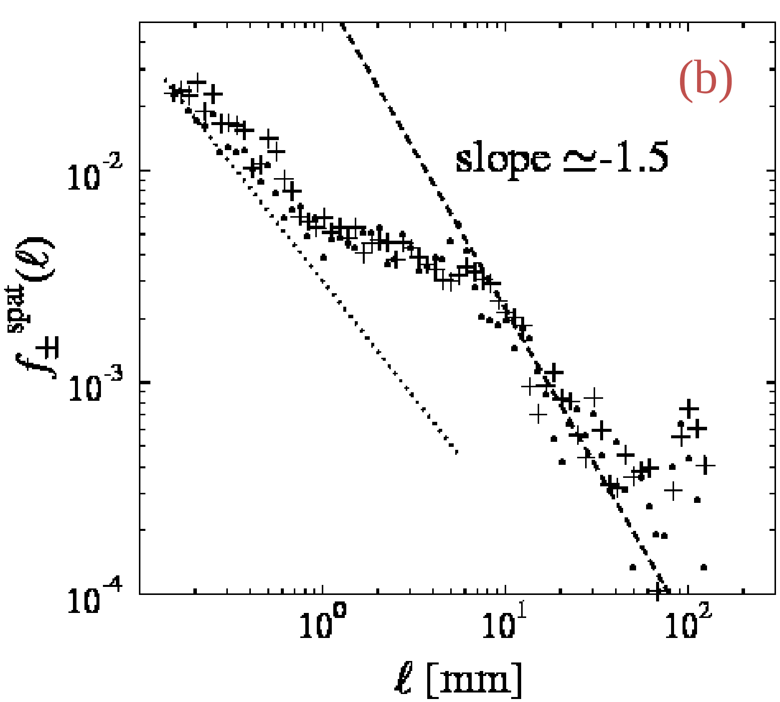

The stationary spatial first-return distributions $f^{spat}(l)$.

Theory : Asymptotically $1+\theta^{temp} = 1.666$ and $1+\theta^{spat} = 1.5$

Demonstration of KPZ dynamics
Height-fluctuation distributions

The probability distribution for local fluctuations of the position around its mean value is given by

$$P\Big(\frac{h(x,t_2)-h(x,t_1)-(t_2-t_1)\langle\partial_t h\rangle}{A_q(t_2-t_1)^{1/3}} \le s\Big) = F_q(s),$$

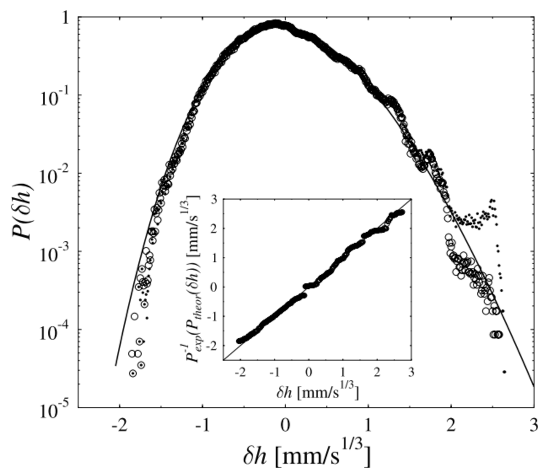

Fig. 3. Height-fluctuation distribution for horizontal fronts in the transient ($w \sim t^{1/3}$) regime, and a fit by a (scaled and shifted) theoretical distribution f_1. A theoretical inversion of the measured distribution is shown in the inset. The dots denote the measured data and the circles the data with an avalanche suppressed.

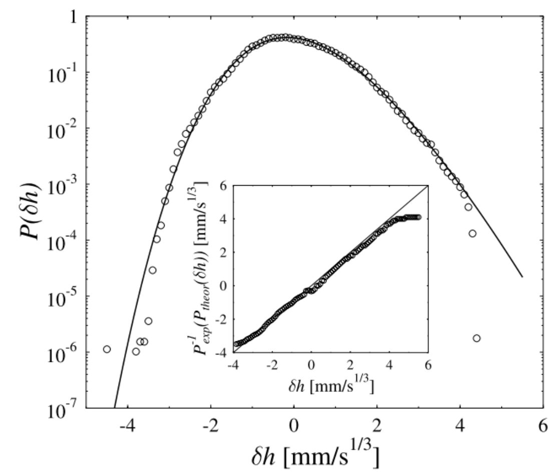

Fig. 6. Height-fluctuation distribution for horizontal fronts in the saturated regime, and a fit by a (scaled) f_0 distribution.

Demonstration of KPZ dynamics

Non-linear term

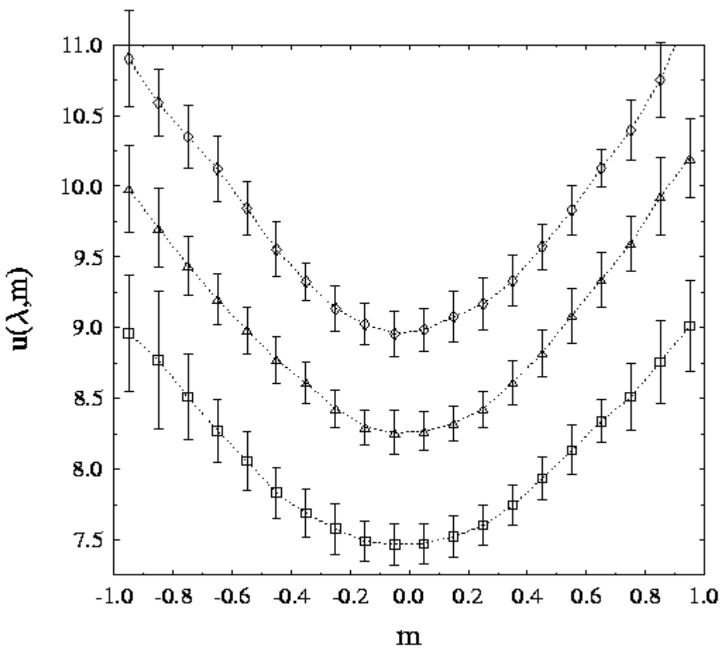

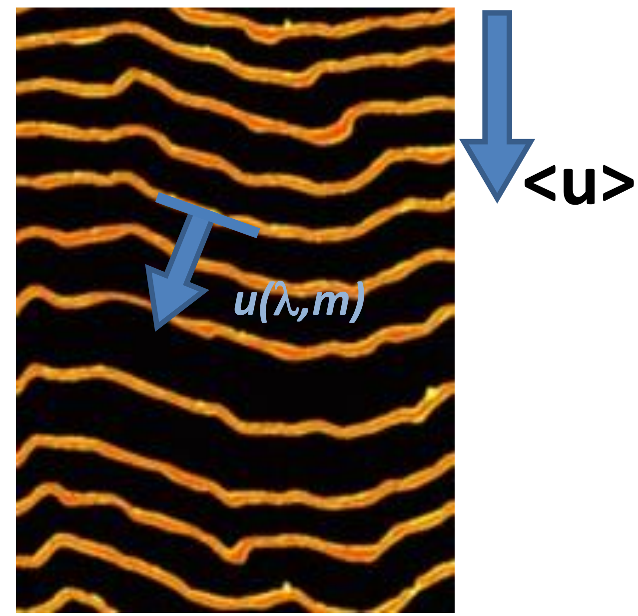

The slope dependent velocity *u(λ,m)* vs. local slope *m* for three different average velocities <*u*>.

Demonstration of KPZ dynamics

Columnar defect

Even a thin columnar defect in a substrate will affect the interface propagating in that substrate. A convenient control parameter of the problem, which determines the size and nature of the effect, is the difference in driving in the defect and elsewhere in the substrate.

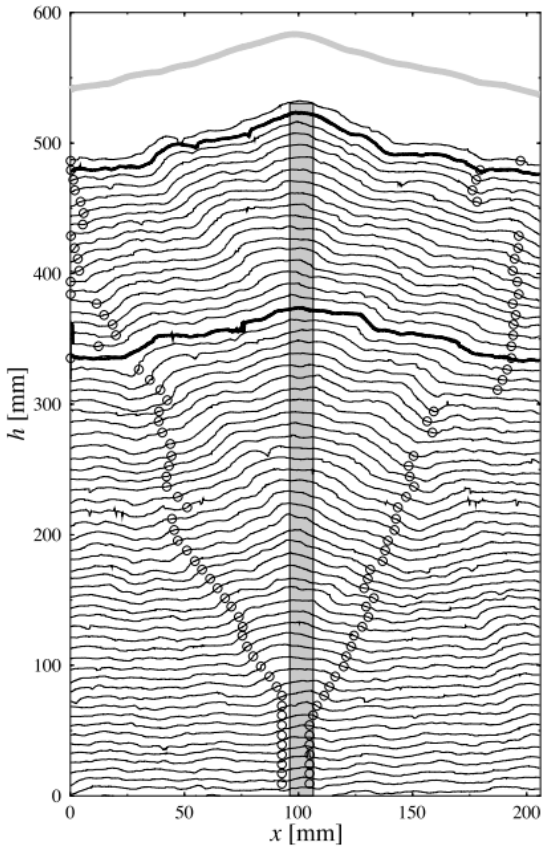

FIG. 4. Successive fronts with a time difference of 0.5 s for the concentration difference $\Delta C = 0.327$. Also marked are the stripe with enhanced concentration of potassium nitrate, the fronts between which the average profile is determined (thick lines), the height of the final profile, and the average shape of the profile.

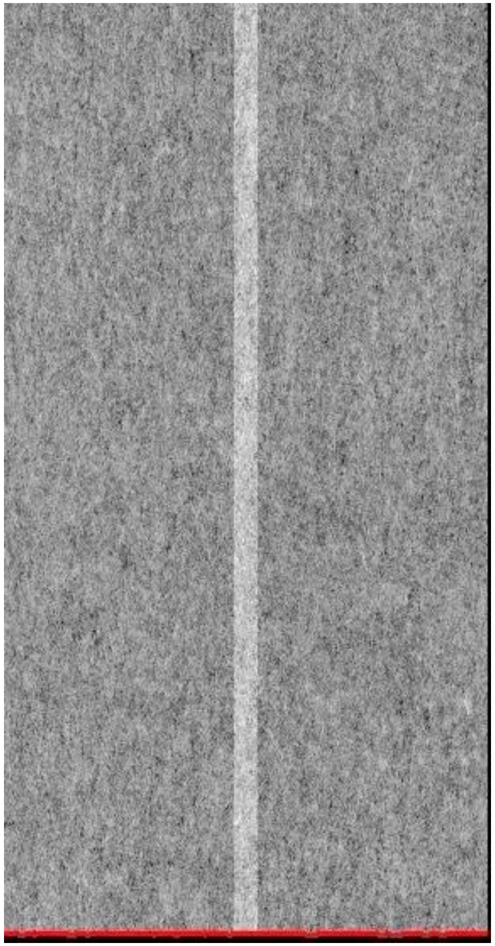

Demonstration of KPZ dynamics

Columnar defect

The **difference in the shape of the front profiles** for enhanced vs reduced driving in the defect **clearly demonstrates the existence of a Kardar-Parisi-Zhang-type nonlinear term** in the effective evolution equation for the slow-combustion fronts. We also find that slow-combustion fronts display a faceted form for large enough enhanced driving, and that there is a corresponding increase then in the average front speed.

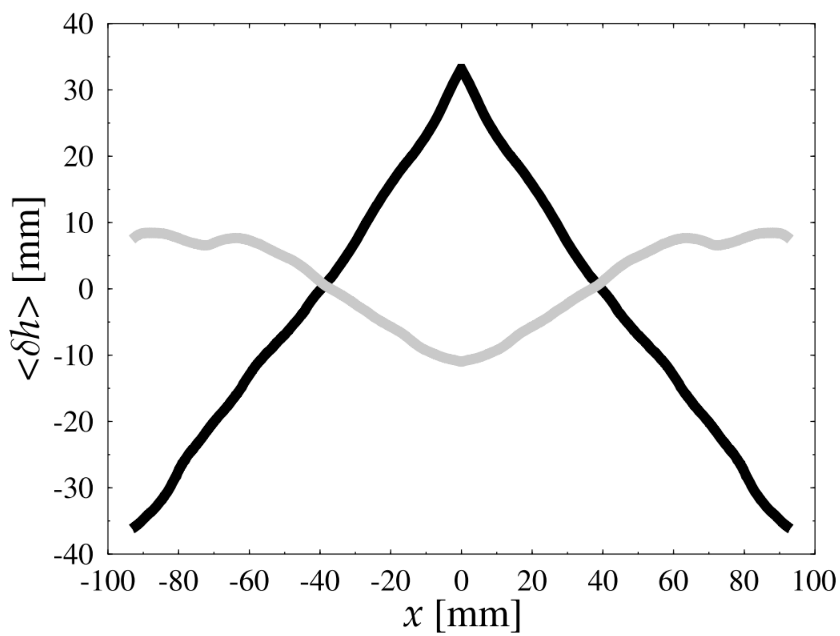

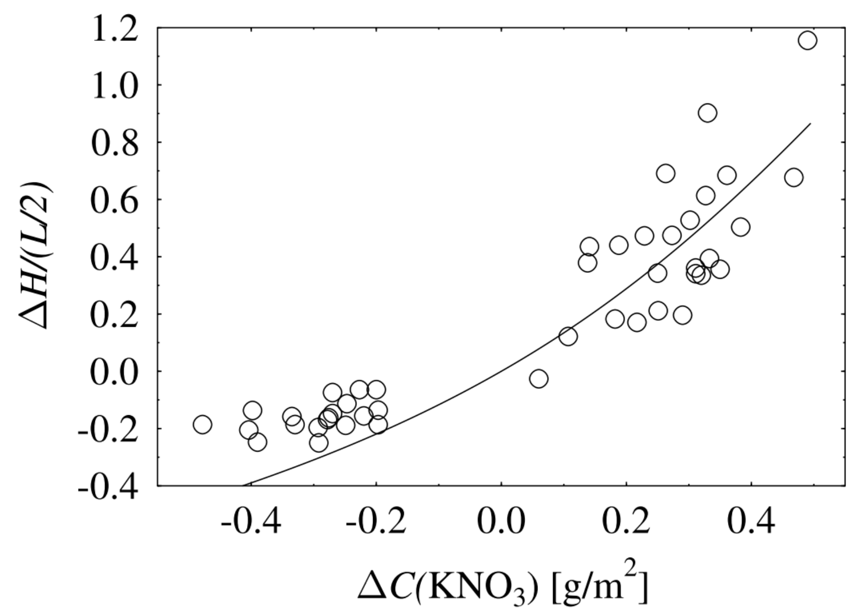

KPZ parameters

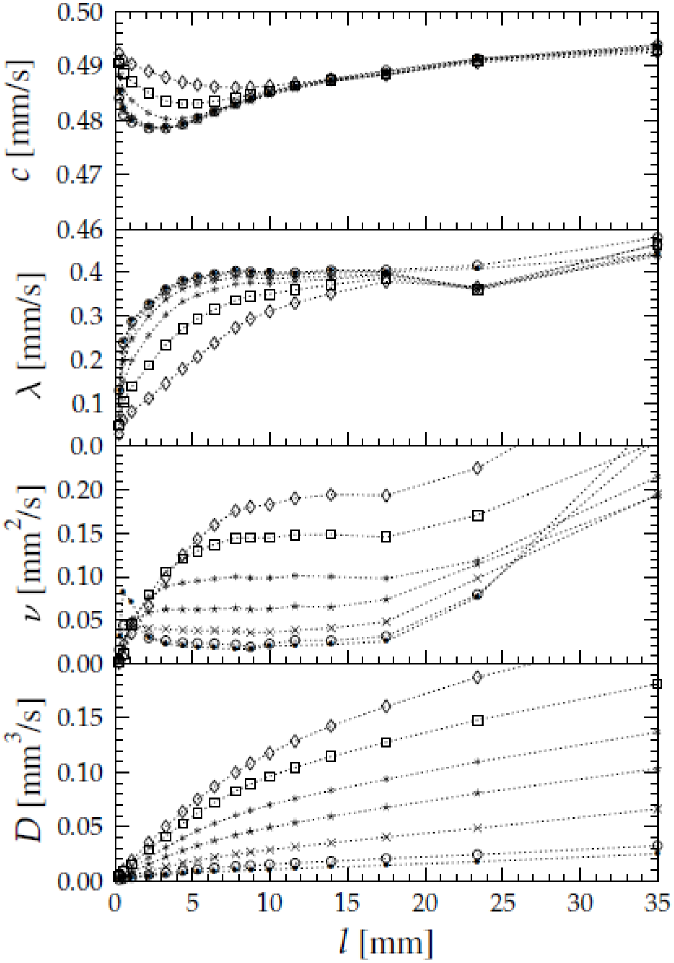

FIGURE 6.5 Model parameters c, λ, ν and D determined by the inverse method and averaged over 18 burns of the 80 $\mathrm{g/m^2}$ copier-paper, as functions of the cutoff length ℓ for $\tau = 0.4\,(\cdot)\ \ldots\ 25.6\,(\diamond)$ s.

Coefficients of the KPZ-equation:

$$\frac{\partial h}{\partial t} = \nu \nabla^2 h + \frac{\lambda}{2}(\nabla h)^2 + c + \eta(x,t)$$

with noise

$$\langle \eta(x,t)\,\eta(x',t') \rangle = 2D\delta(x-x')\delta(t-t')$$

were calculated using an inverse method as a function of coarse graining level l and time step $\boldsymbol{\tau}$.

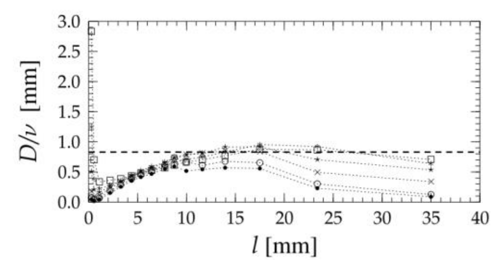

.6 Measured D/ν as a function of cutoff length ℓ for the 80 $\mathrm{g/m^2}$ copier-
rns.

KPZ parameters

TABLE 6.4 Measured average values for KPZ coeffients and the ratio D/ν. For the slow-combustion fronts $l = 11.6 \ldots 17.6$ mm and $\tau = 0.4$ s, and for the magnetic flux fronts $l = 11.2 \ldots 19.6$ µm and $\tau = 0.5$ s, were used as the coarse-graining scales for c and λ. The scaled ν and the D/ν ratio were determined for $\ell = 17.5$ mm and $\tau = 25.6$ s (copier-paper), and $\ell = 17.6$ mm and $\tau = 1.6$ s (lens-paper). The D/ν ratio for the magnetic flux was determined for $\ell = 22.4$ µm and $\tau = 3.5$ s.

Coefficient	Inverse method			Slope-dependent velocity		
	Copier	Lens	Flux $\times 10^{-3}$	Copier	Lens	Flux $\times 10^{-3}$
c [mm/s]	0.49(2)	9.2(5)	27.0(1)	0.485(2)	9.1(2)	27.1(2)
λ [mm/s]	0.40(2)	4.1(2)	15.9(8)	0.37(3)	5.1(2)	17.4(2)
$\nu \left(\frac{\tau}{\Delta t}\right)^{-1/3}$ [mm^2/s]	0.049(3)	2.0(1)	–	–	–	–
D/ν [mm]	0.83(5)	4.6(1.1)	6(3)	–	–	–

Short range behaviour

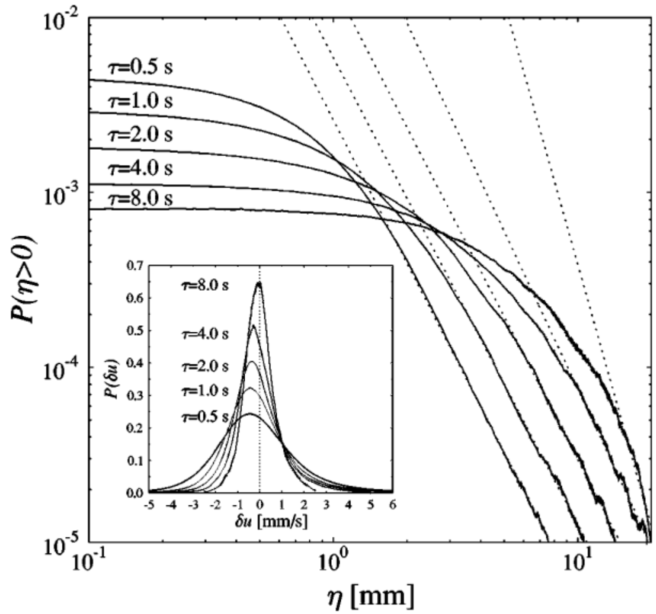

FIG. 9. The noise amplitude distribution $P(\eta>0)$ averaged over 35 burns of the 9.1 gm^{-2} lens paper with an average velocity >8.4 mm/s. The distribution was calculated for time intervals $\tau=0.5$, 1.0, 2.0, 4.0, and 8.0 s shown in the figure. The linear fits have slopes -2.71, -2.67, -2.72, -2.99, and -4.97, left to right. The inset shows the local velocity fluctuation distributions for the same time intervals τ.

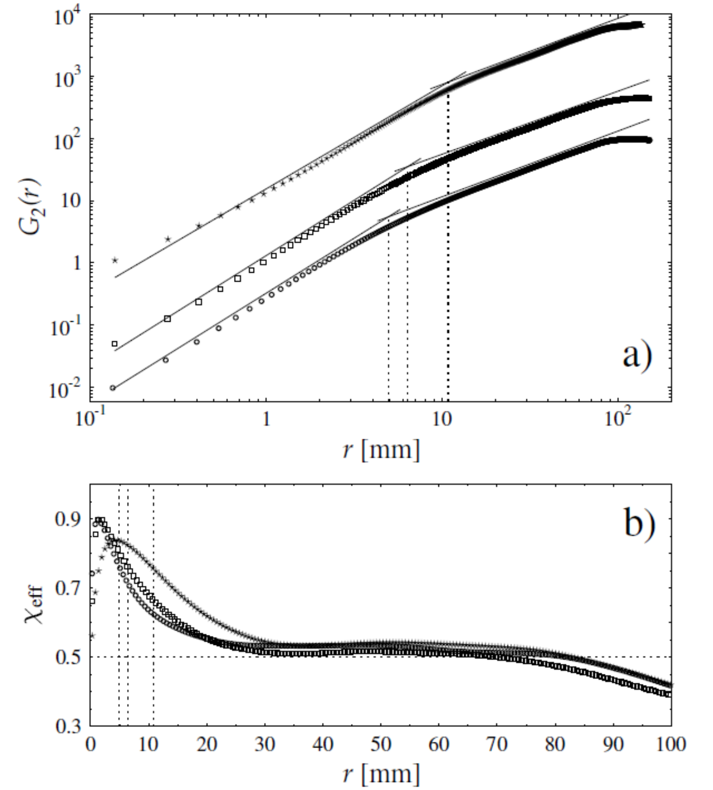

FIGURE 4.2 (a) Spatial correlation functions $G_2(r)$ for three paper grades, and (b) the resulting effective exponents. Crossover scales from the short-range regimes to the asymptotic scaling regimes are marked with dotted lines.

Short range behaviour

Multiscaling

$$C_q(r,\tau) = \langle[\delta h(x,t) - \delta h(x+r,t+\tau)]^q\rangle_{x,t} \ ,$$

$$G_q(r) \equiv C_q(r,0) \sim r^{q\chi_q}$$

$$C_q(\tau) \equiv C_q(0,\tau) \sim \tau^{q\beta_q}$$

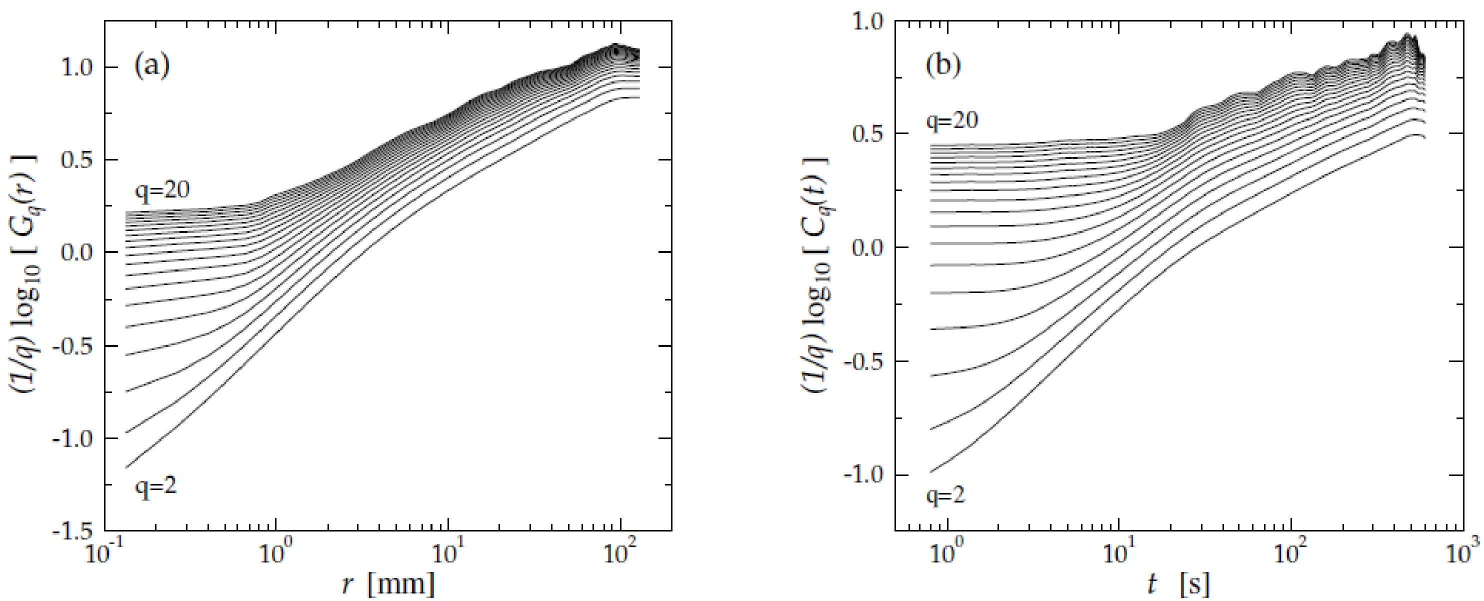

FIGURE 6.3 The (a) spatial and (b) temporal qth order correlation functions $G_q(r)$ and $C_q(t)$ averaged over 10 burns for the $70\,\mathrm{g/m^2}$ copier paper and 20 burns for the $80\,\mathrm{g/m^2}$ copier paper, respectively.

Short range

$$\eta_{\mathrm{eff}}(x,t) \equiv \delta h(x,t+\tau) - \delta h(x,t),$$

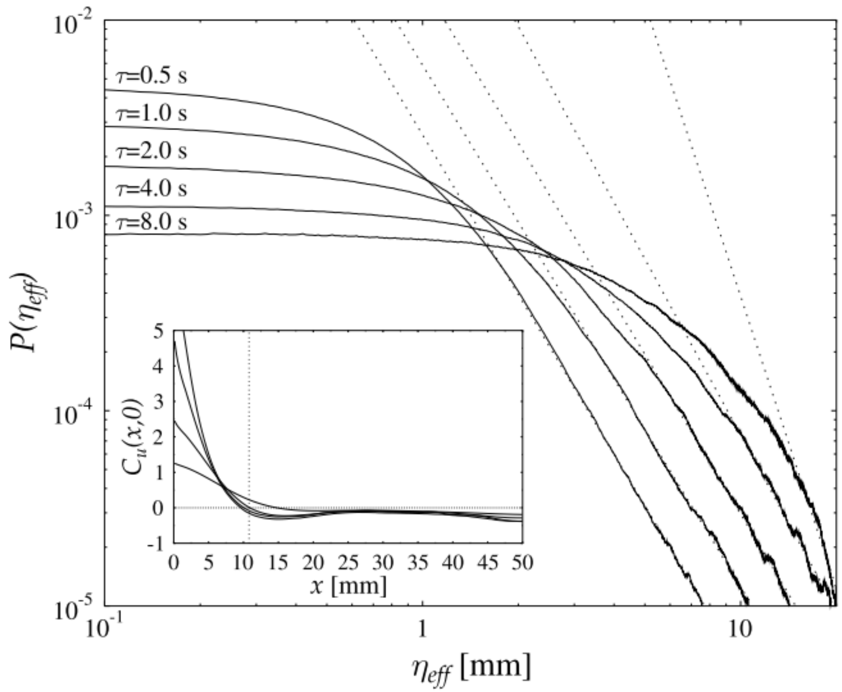

FIGURE 4.7 The noise amplitude distribution $P(\eta_{\mathrm{eff}})$ for slow-combustion fronts in lens paper determined for time steps $\tau = 0.5, 1.0, 2.0, 4.0$, and 8.0 s. The inset shows the spatial correlations of the velocity fluctuations in the same samples.

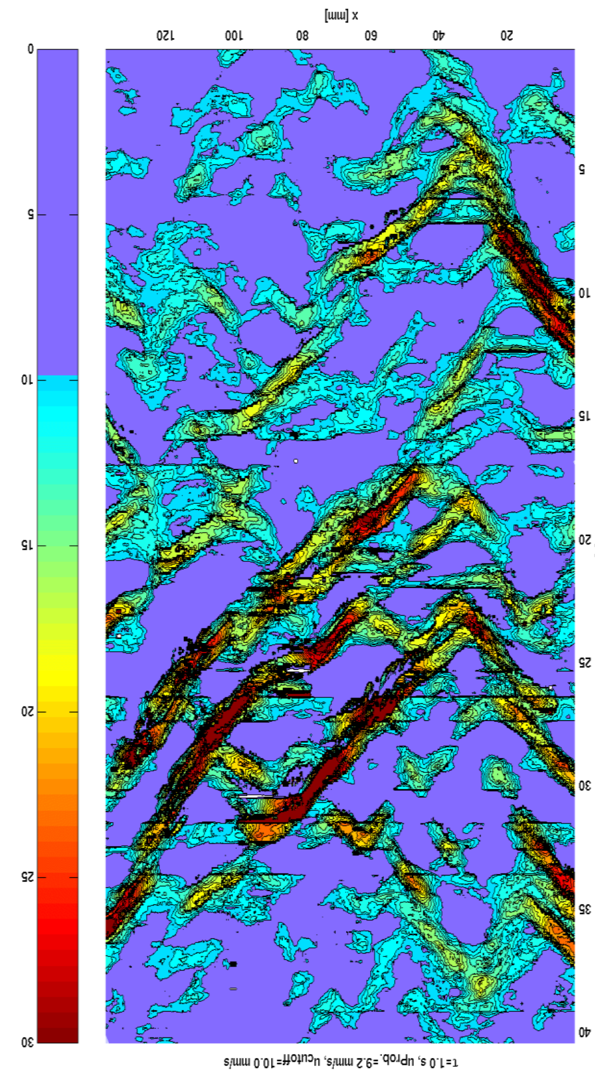

Simulations

Numerical solution of KPZ-equation was achived by using the Euler's method solution of the finite difference equation

$$h_i^{n+1} = h_i^n + \frac{\Delta t}{\Delta x^2}\Big[\nu_0(h_{i+1}^n + h_{i-1}^n - 2h_i^n) + (\lambda_0/6)[(h_{i+1}^n - h_i^n)^2$$
$$+(h_{i+1}^n - h_i^n)(h_i^n - h_{i-1}^n) + (h_i^n - h_{i-1}^n)^2]\Big] + \Delta t\, c_0 + \sqrt{\frac{2D_0\Delta t}{\Delta x}}\,\xi(i, h_i^n),$$

The **nominal values of the parameters $\square_0$ and $\square_0$** were obtained by an inverse method **from our experimental data** as described above. The nominal values for c_0 and D_0 were fixed by comparing the velocity distributions from simulations and experiments. **The noise matrices were obtained from paper samples** of the same grades as used in the experiments.

Simulations

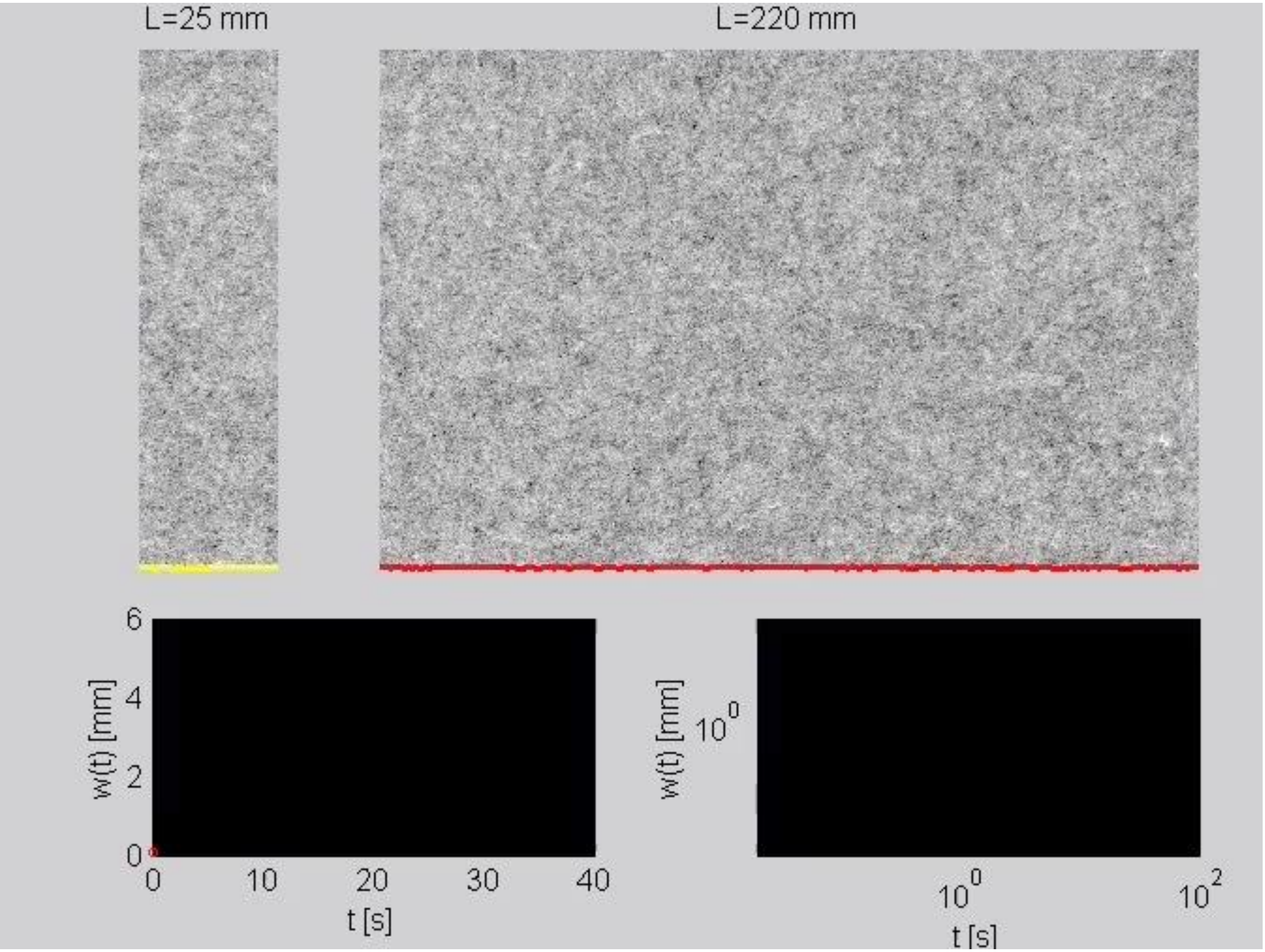

Simulations

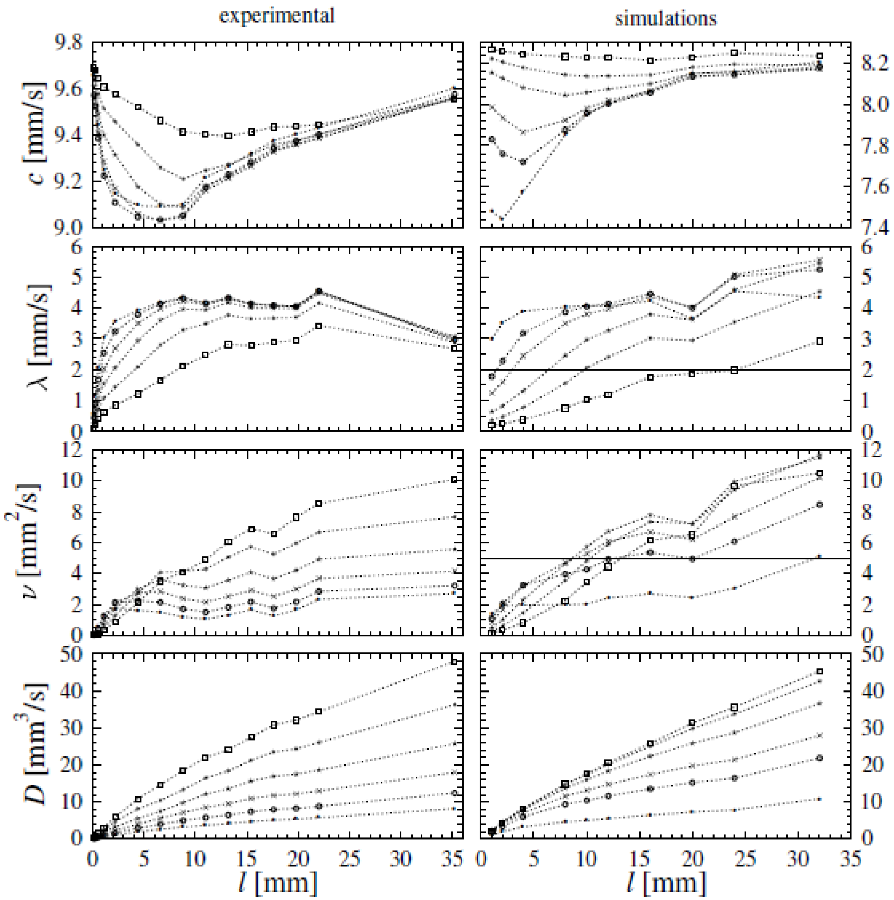

FIGURE 5.1 The effective parameters for τ= 0.2(.), 0.4(○), 0.8(×), 1.6(⋆), 3.2(*) and 6.4(□) s of the KPZ equation as determined by the inverse method. On the left are the experimental values and on the right the effective values determined from the simulated fronts produced by our 'best simulation model'. The nominal values λ_0 and ν_0 are indicated by the horizontal lines.

Simulations

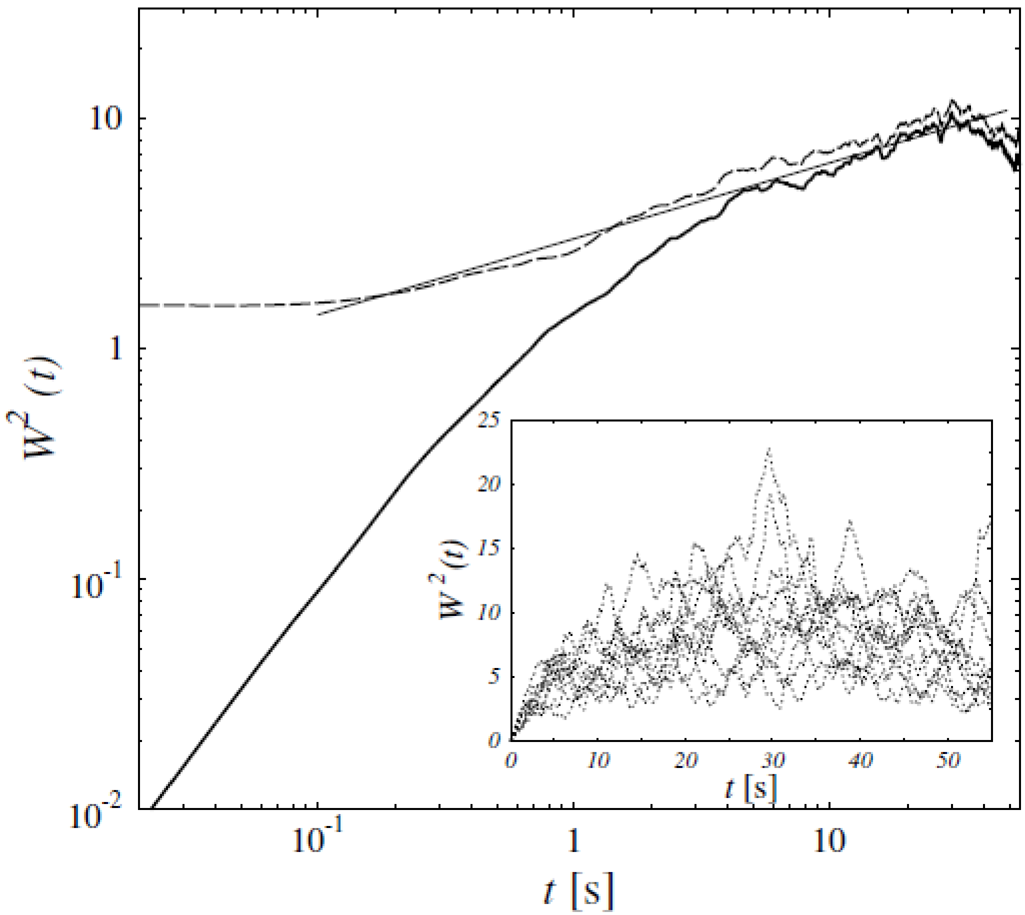

FIGURE 5.2 The average front widths w^2 as functions of time for ten lens-paper simulations. The result for a flat initial condition is plotted with a thick solid line, and with a dashed line for rough initial conditions. The inset displays the magnitude of fluctuations, showing the individual results for ten realizations of noise.

Simulations

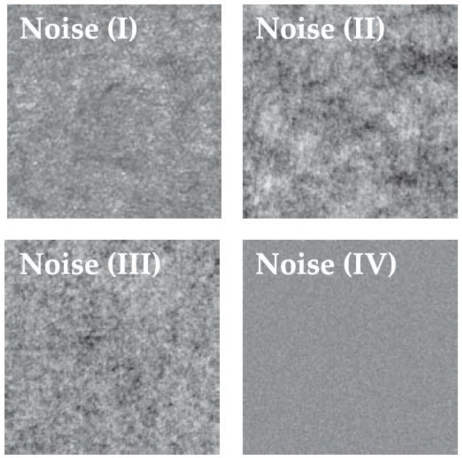

Fig. 1. 30×30 mm^2 samples of the noise used in the simulations. Noise (I) is an optically scanned image of lens paper, and noise (II) and noise (III) are β-radiographs of copier papers. Noise (IV) is generated by disordering noise (I).

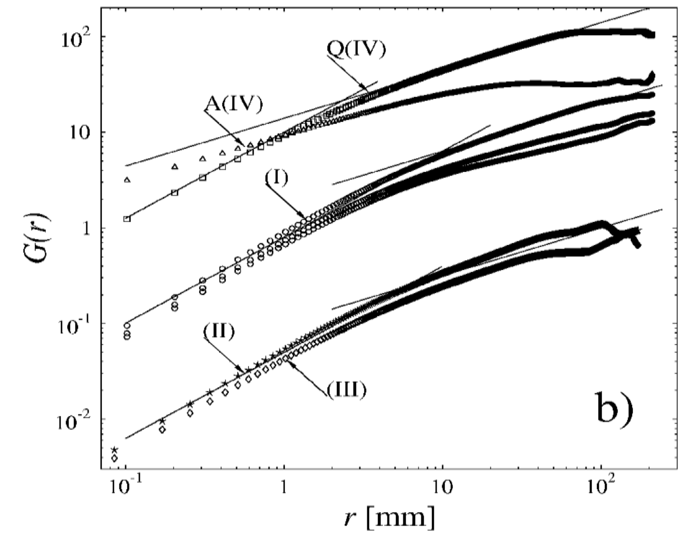

* **Simulations using real paper structure as an input noise.**

* **Input parameters for KPZ equation measured from experiments.**

* **Similar asymptotic KPZ scaling properties as in experiments.**

* **Anomalous short range scaling was a consequence of the short-range correlated paper structure.**

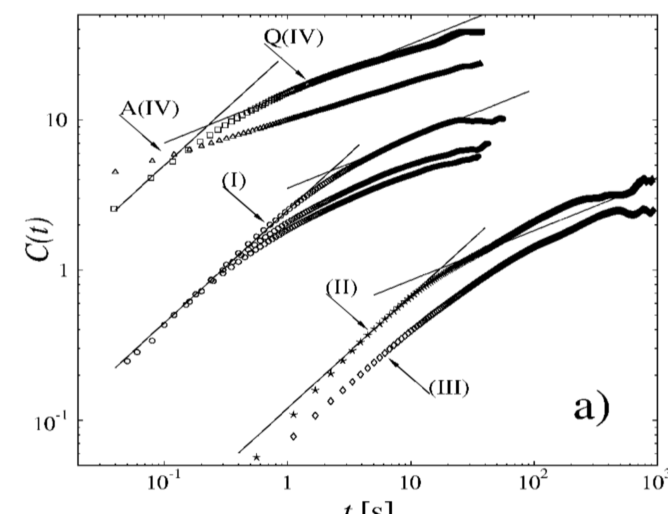

Simulations

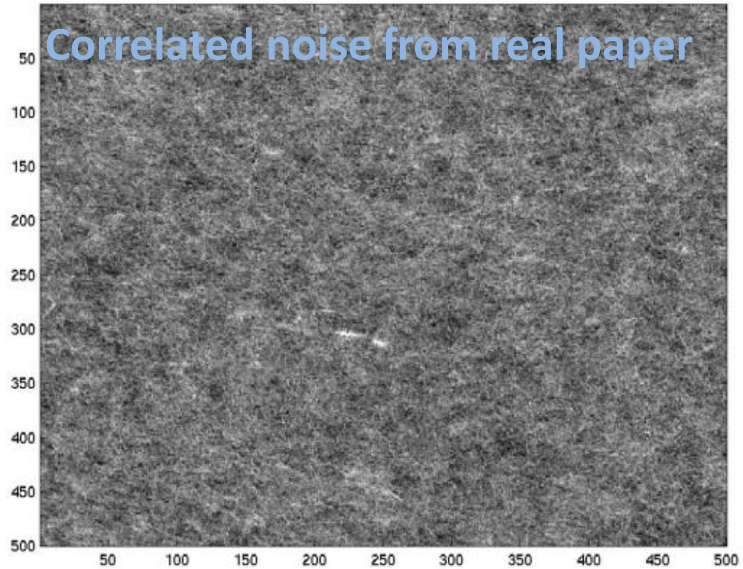

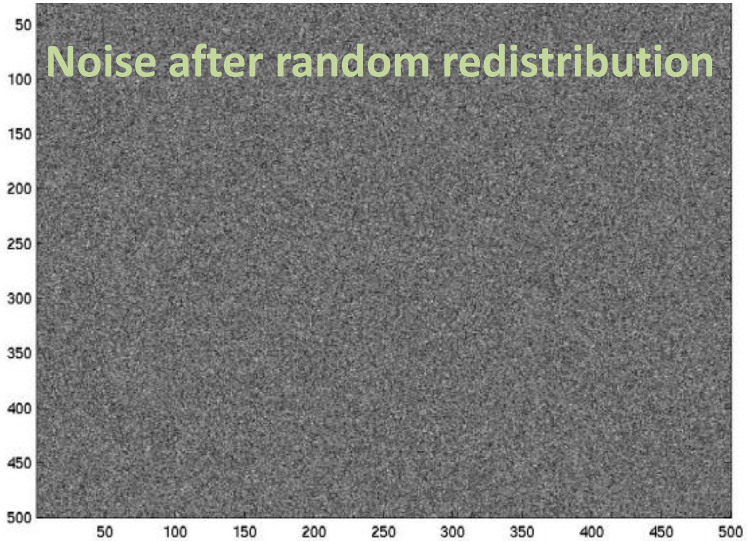

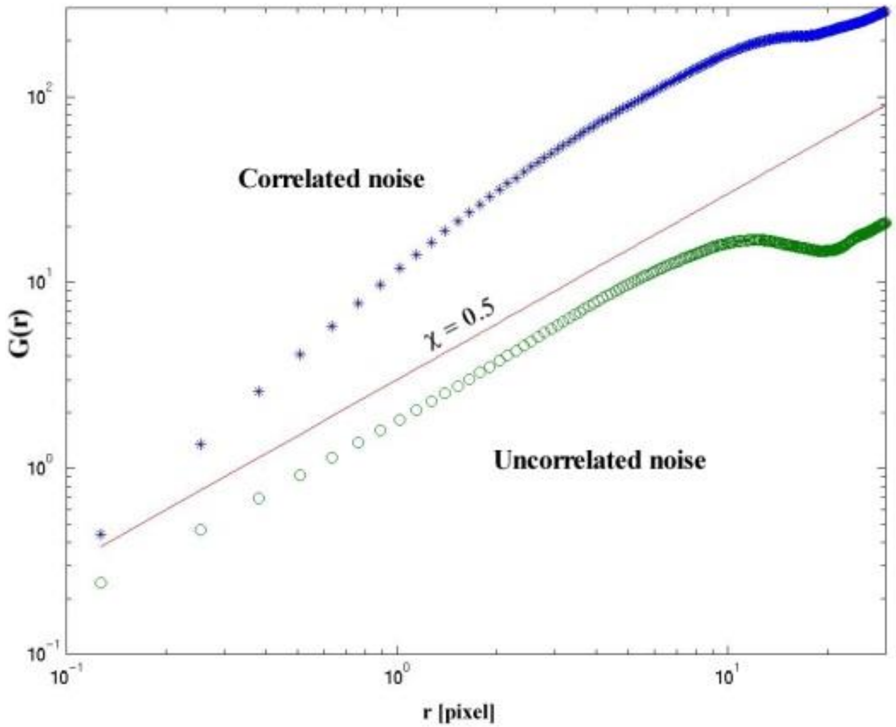

Spatial correlation functions ***G(r)***
for both noises from KPZ simulations.

Conclusions

* **Experiments :** well propagating fronts in paper
  - **Extensive averaging over noise is necessary**

* **Asymptotic behaviour** : **<u>KPZ universality class</u>** with white noise
  - correlation functions (χ , β)
  - universal coupling constant (g*)
  - persistence (θ)

* Anomalous **short range behaviour** below cross-over:
  - short-range **correlations** in noise => **higher apparent scaling exponents**
  - **dynamic effects** ‘amplify’ quenched noise in temporal direction

*** Simulations of the KPZ equation** with relevant noise and parameters show similar asymptotic and short range behaviour than experiment.

The latest achievements

Preparing 8 meter long paper sample

The latest achievements

Experiment of 6 meter long paper sample

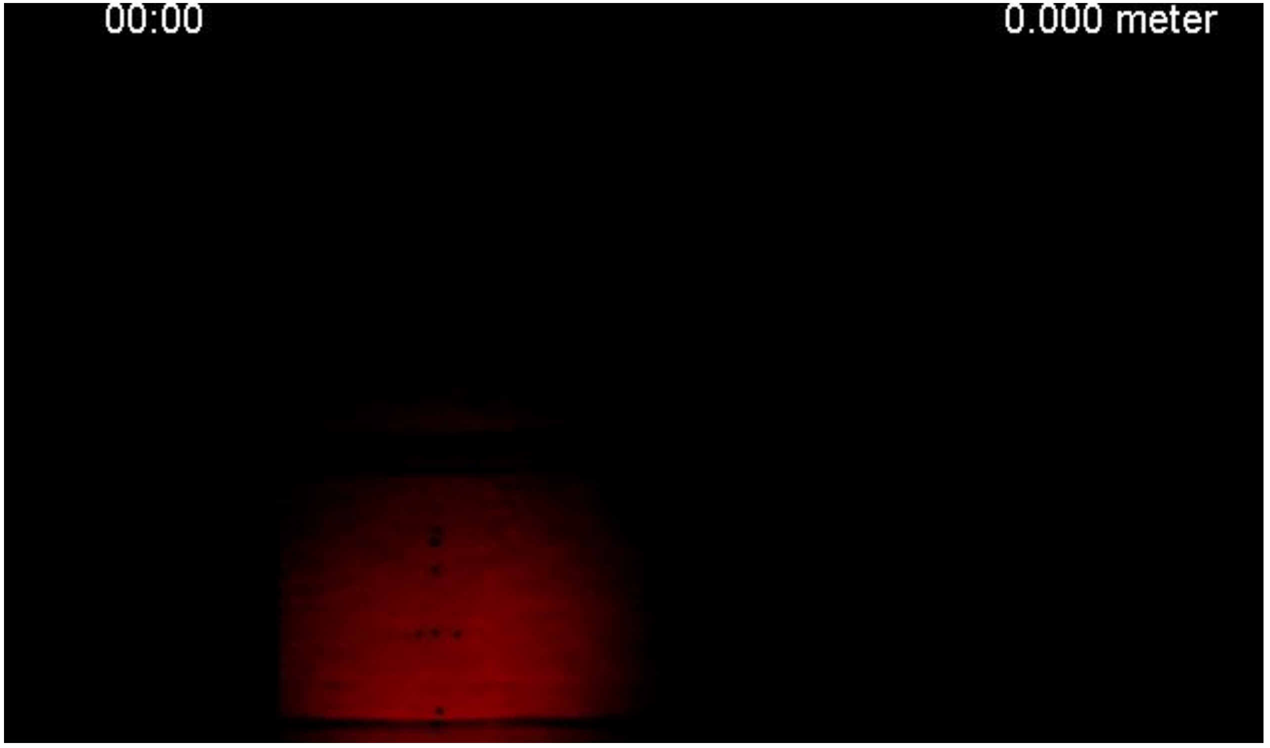

The latest achievements

Preliminary results for 6 meter long paper

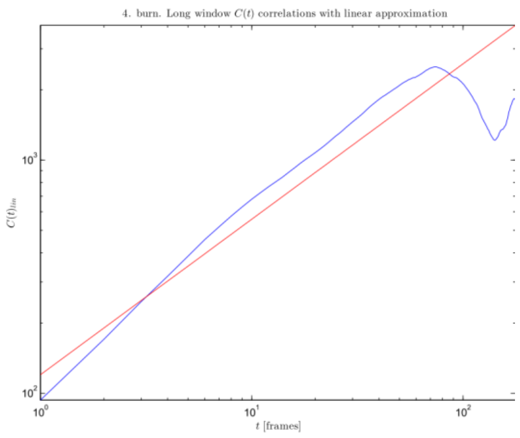

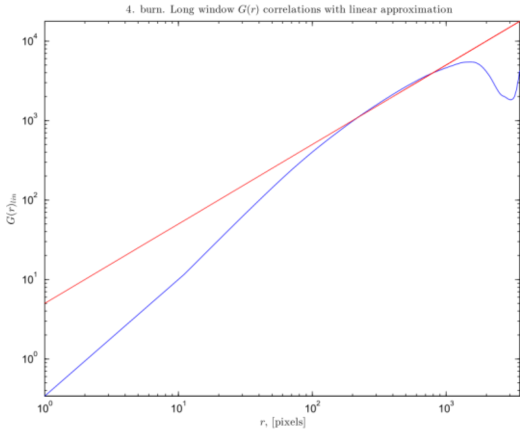

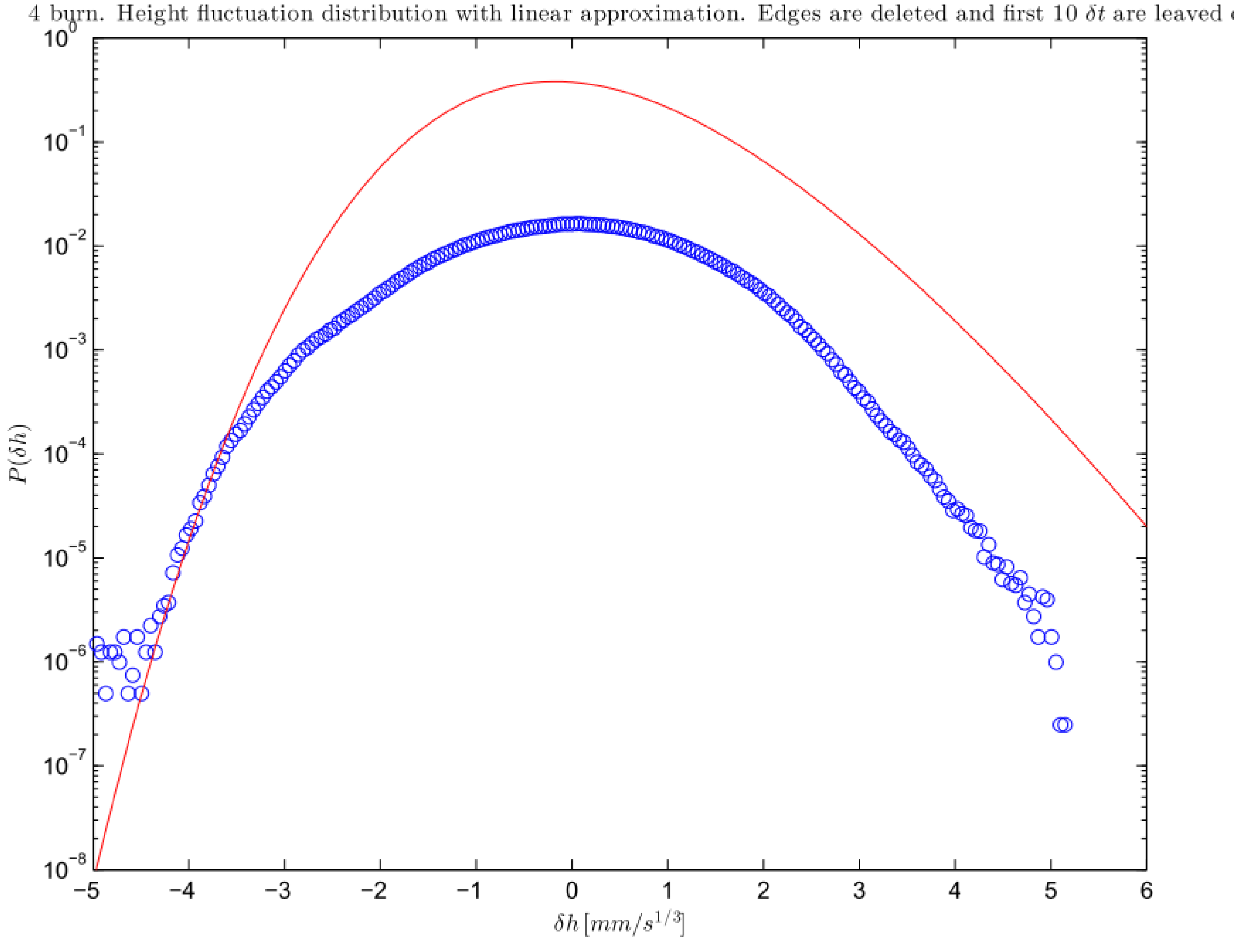

Future work

- New paper grade with better formation and without coating layer
- Wider paper sample to get more statistics from transient region
- Open access to experimental data
-

Future work

Pinning transition

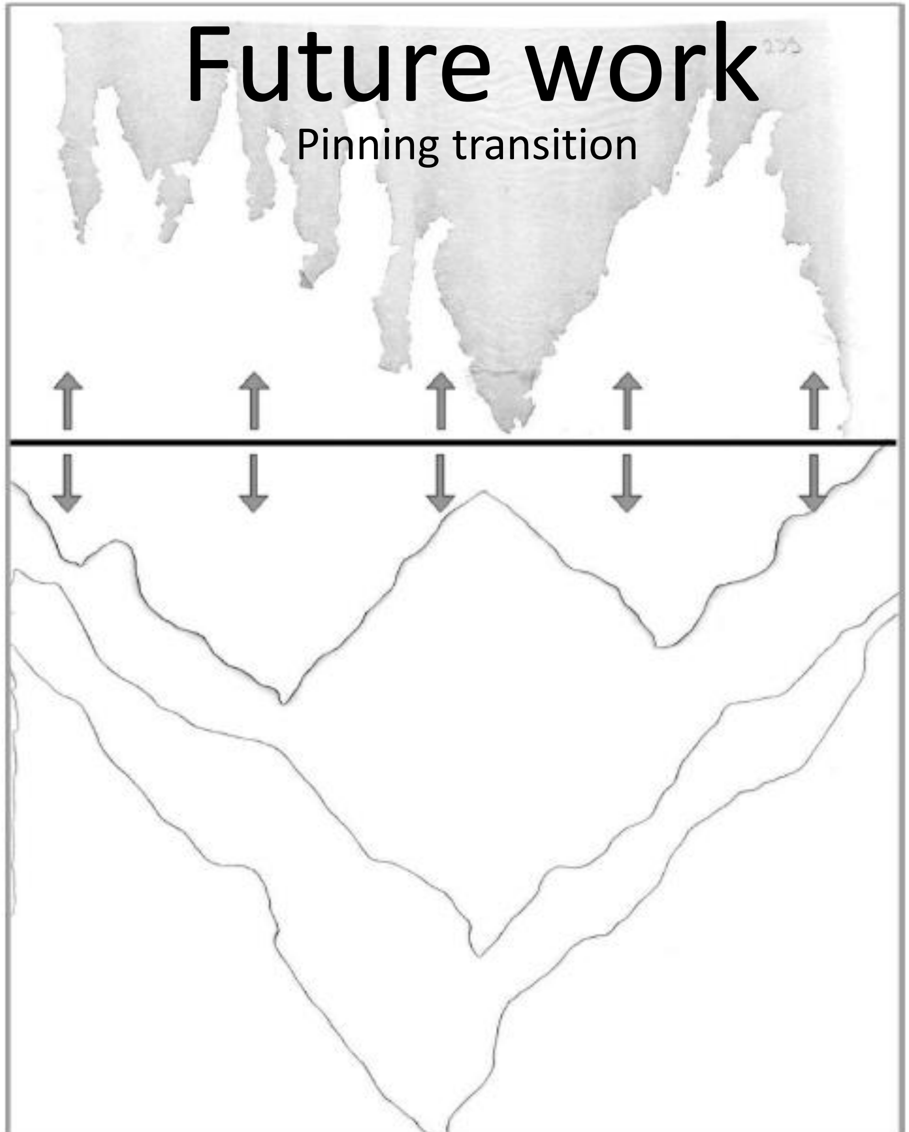

FIGURE 6.1 Pinned interfaces. The lower configurations are for copier paper samples and the uppermost configuration for a lens paper sample with a low KNO_3 concentration.

Thank you for your attention